

PHYSICO-CHEMICAL ANALYSIS OF INORGANIC SYSTEMS

Investigation of the Chemical Interaction in the Sb_2Te_3 –InSe System and the Properties of the Obtained Phases

I. I. Aliev^{a, *}, N. A. Mamedova^a, F. M. Sadygov^b, N. M. Sadygov^c, and I. G. Melikova^a

^aNagiev Institute of Catalysis and Inorganic Chemistry, National Academy of Sciences of Azerbaijan, Baku, Az1143 Azerbaijan

^bKhalilov Baku State University, Baku, Az1143 Azerbaijan

^cInstitute of Geology, National Academy of Sciences of Azerbaijan, Baku, Az1143 Azerbaijan

*e-mail: iradam@rambler.ru

Received December 11, 2019; revised May 29, 2020; accepted May 30, 2020

Abstract—The interaction in the Sb_2Te_3 –InSe system was studied and the T – x phase diagram was constructed by integrated methods of physicochemical analysis (differential thermal, X-ray powder diffraction, and microstructural analyses) and also by microhardness and density measurements. It was found that the Sb_2Te_3 –InSe system is a quasi-binary section of the ternary reciprocal system $\text{Sb, In} \parallel \text{Se, Te}$. In the Sb_2Te_3 –InSe system, compounds $\text{InSb}_2\text{SeTe}_3$ and $\text{In}_3\text{Sb}_2\text{Se}_3\text{Te}_3$ form, which incongruently melt at 525 and 600°C, respectively. It was found that the regions of solid solutions based on Sb_2Te_3 and InSe extend to 3 and 2 mol %, respectively. The compounds Sb_2Se_3 and InSe form a eutectic with the coordinates 20 mol % InSe and 510°C. The temperature dependences of the electrical conductivity and thermal emf of the solid solutions $(\text{Sb}_2\text{Te}_3)_{1-x}(\text{InSe})_x$ ($x = 0.01, 0.02, \text{ and } 0.03$).

Keywords: phase formation, eutectic, quasi-binary, solid solution, electrical conductivity

DOI: 10.1134/S0036023620100010

INTRODUCTION

The development of multifunctional materials with given properties is based on studying the composition–property diagrams of multicomponent systems. It is known that indium and antimony chalcogenides and alloys based on them have optical [1–6], photoelectric [7–10], thermoelectric, and luminescent properties [11–17] and are widely used in the electronics industry: they are also of interest as semiconductors. The phase diagrams of many systems containing indium and antimony [18–24] and some physicochemical properties of their alloys [25–27] were investigated. Therefore, the development of materials based on antimony and indium chalcogenides is an urgent problem and requires the fundamental search.

The purpose of this work was the investigation of the chemical interaction in the Sb_2Te_3 –InSe system and also the search for new phases and solid solutions.

Donnay and Ondik determined [28] that the compound Sb_2Te_3 has a crystal structure of the Bi_2Te_3 type and crystallizes in the rhombohedral system with the unit cell parameters $a = 4.264 \text{ \AA}$ and $c = 30.42 \text{ \AA}$ in the space group $R3m$.

The crystal structure of the compound Sb_2Te_3 was also studied by Kuznetsov and Palkina [29], who reported that the compound Sb_2Te_3 crystallizes in the rhombohedral system with the unit cell parameters $a =$

4.262 \AA and $c = 30.450 \text{ \AA}$ in the space group $R3m$, D_{3d}^5 . The data of the works [28] and [29] agree well with each other.

The compound InSe melts congruently at 660°C, belongs to the structural type of GaSe, and crystallizes in the hexagonal system with the unit cell parameters $a = 4.04 \text{ \AA}$ and $c = 16.92 \text{ \AA}$ [30].

EXPERIMENTAL

Alloys in the system were synthesized by direct melting of the components Sb_2Te_3 and InSe in ampules in the temperature range 700–900°C with subsequent slow cooling in switched-off furnace mode. To reach the equilibrium state, the samples were annealed at 500°C for 140 h.

Differential thermal analysis of samples was performed with a Termoskan-2 thermal recorder at a heating rate of 9 deg/min. The X-ray powder diffraction patterns were recorded with a D2 Phaser diffractometer (CuK_α radiation). The microhardness was measured with a PMT-3 microhardness meter at loads chosen by studying the microhardness of each phase. The microstructure of the alloys was investigated with a MIM-8 microscope. Polished sections of the alloys were etched with a solution of 10 mL of concentrated HNO_3 in H_2O_2 in the ratio 1 : 2 for 15–20 s. The den-

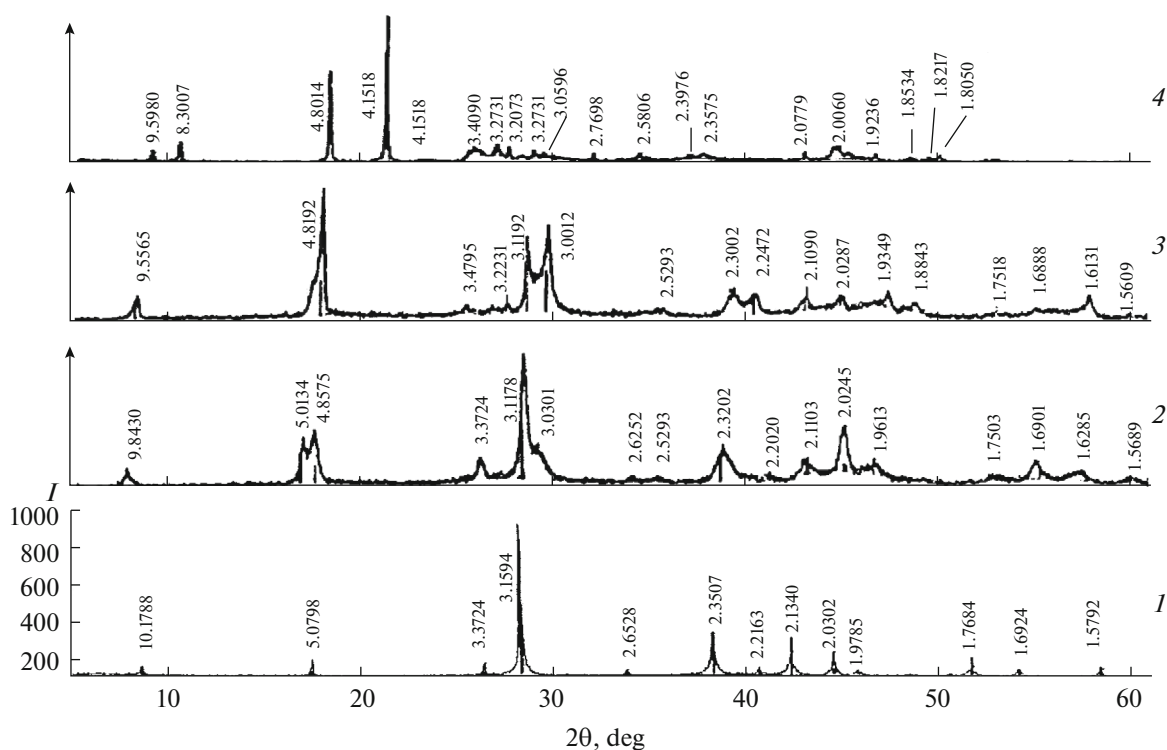


Fig. 1. X-ray powder diffraction patterns of alloys in the Sb_2Te_3 – InSe system: (1) Sb_2Te_3 , (2) $\text{InSb}_2\text{SeTe}_3$, (3) $\text{In}_3\text{Sb}_2\text{Se}_3\text{Te}_3$, and (4) InSe .

sity was determined by pycnometry with toluene as a displacement liquid. The electrical conductivity of the alloys in the system was studied by known compensation methods [31]. The elemental percentages in the compounds $\text{InSb}_2\text{SeTe}_3$ and $\text{In}_3\text{Sb}_2\text{Se}_3\text{Te}_3$ were analyzed with a Jeol JSM 6610–ICP–MS 7700 scanning electron microscopy. The elemental percentages within the range $n \times 10^{-8}$ – $n \times 10\%$ determined with a mass spectrometer.

RESULTS AND DISCUSSION

Sb_2Te_3 -rich alloys in the Sb_2Te_3 – InSe system are of silver color, brittle, and layered and acquire a black shade with increasing InSe content. They are resistant to air and water, but are decomposed by concentrated mineral acids (HNO_3 , H_2SO_4), whereas organic solvents do not affect them. Equilibrium alloys were investigated by methods of physicochemical analysis.

The differential thermal analysis of alloys in the Sb_2Te_3 – InSe system showed that the thermal curves have two or three thermal events each. The microstructural analysis demonstrated that there are limited homogeneous regions based on the initial components. In the system at room temperature, the solubilities based on Sb_2Te_3 and InSe are 3 and 2 mol %, respectively; the obtained alloys containing 50 and 75 mol % InSe are also single-phase.

In the Sb_2Te_3 – InSe system, new compounds, $\text{InSb}_2\text{SeTe}_3$ and $\text{In}_3\text{Sb}_2\text{Se}_3\text{Te}_3$, form, which incongruently melt at 525 and 600°C, respectively.

X-ray powder diffraction analysis was carried out to confirm the results of the differential thermal and microstructural analyses. Figure 1 presents the X-ray powder diffraction patterns of the alloys containing 50 and 75 mol % InSe and the initial components. It was determined that the X-ray powder diffraction patterns of the alloys containing 50 and 75 mol % InSe have diffraction lines that do not correspond in intensity and position of interplanar distances to the diffraction lines of the initial components. The compound $\text{InSb}_2\text{SeTe}_3$ crystallizes in the tetragonal system with the unit cell parameters $a = 19.686 \text{ \AA}$, $c = 13.490 \text{ \AA}$, $\rho_{\text{pyc}} = 6.18 \text{ g/cm}^3$, and $\rho_{\text{X-ray}} = 6.25 \text{ g/cm}^3$. The compound $\text{In}_3\text{Sb}_2\text{Se}_3\text{Te}_3$ is isostructural to $\text{InSb}_2\text{SeTe}_3$ and crystallizes in the tetragonal symmetry with the unit cell parameters $a = 19.113 \text{ \AA}$, $c = 12.892 \text{ \AA}$, $\rho_{\text{pyc}} = 5.88 \text{ g/cm}^3$, and $\rho_{\text{X-ray}} = 5.96 \text{ g/cm}^3$. Table 1 presents the X-ray powder diffraction data on the compounds $\text{In}_3\text{Sb}_2\text{Te}_6$ and InSb_2Te_4 .

The spectra and microstructures of the compounds $\text{InSb}_2\text{SeTe}_3$ and $\text{In}_3\text{Sb}_2\text{Se}_3\text{Te}_3$ were recorded with a scanning electron microscope and shown in Figs. 2 and 3.

Table 1. Interplanar distances d (hkl) and the line intensities in the X-ray powder diffraction patterns of the compounds $\text{InSb}_2\text{SeTe}_3$ and $\text{In}_3\text{Sb}_2\text{Se}_3\text{Te}_3$

$\text{InSb}_2\text{SeTe}_3$					$\text{In}_3\text{Sb}_2\text{Se}_3\text{Te}_3$				
$I, \%$	$d, \text{Å}$	h	k	l	$I, \%$	$d, \text{Å}$	h	k	l
15	9.8430	2	0	0	19	9.5565	2	0	0
63	5.0134	3	2	1	100	4.8192	4	0	0
69	4.8575	4	0	0	8	3.4795	3	1	3
19	3.3724	0	0	4	13	3.2231	0	0	4
100	3.1178	6	2	0	56	3.1192	6	1	0
25	3.0301	5	3	2	68	3.0012	5	4	0
6	2.6252	6	1	3	6	2.5293	6	1	3
6	2.5293	6	5	0	21	2.3002	5	3	4
30	2.3202	8	3	0	18	2.2472	8	3	0
9	2.2020	8	4	0	21	2.1090	9	1	0
15	2.1103	9	2	1	13	2.0287	8	5	0
38	2.0245	6	5	4	19	1.9347	7	7	0
13	1.9613	10	2	0	9	1.8843	8	2	4
8	1.7503	11	2	1	6	1.7518	8	0	5
16	1.6901	0	0	8	8	1.6888	8	8	0
10	1.6285	3	1	8	19	1.6131	0	0	8
6	1.5689	10	2	5	4	1.5609	12	0	1

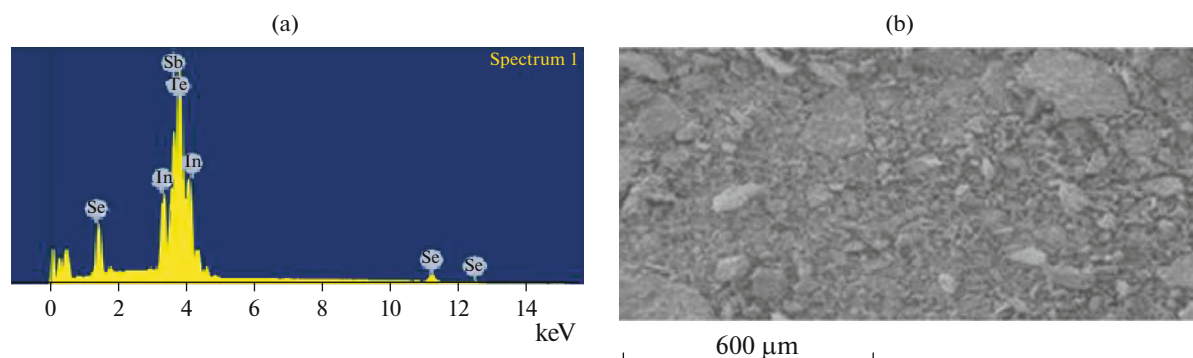
The T – x phase diagram of the Sb_2Te_3 – InSe system was constructed based on the data obtained in this work (Fig. 4).

The liquidus of the system consists of four curves of primary phase separation of α -solid solutions based on Sb_2Te_3 , $\text{InSb}_2\text{SeTe}_3$, and $\text{In}_3\text{Sb}_2\text{Se}_3\text{Te}_3$ and β -solid solution based on InSe . In the system, the cocrystallization of the α -phase and $\text{InSb}_2\text{Te}_3\text{Se}$ ends at the binary eutectic with the coordinates 20 mol % InSe and 510°C . In the concentration range 0–20 mol % InSe , primary crystals of the α -phase precipitate from the liquid; and in the range 40–100 mol % InSe , primary crystals of the β -phase do. In the range 3–50 mol % InSe below the solidus line, two-phase alloys $\alpha + \text{InSb}_2\text{SeTe}_3$ crystallize; in the range 50–75 mol % InSe below the solidus line, two-phase alloys $\text{InSb}_2\text{SeTe}_3 + \text{In}_3\text{Sb}_2\text{Se}_3\text{Te}_3$ do, and in the range 75–98 mol % InSe , two-phase alloys $\text{In}_3\text{Sb}_2\text{Se}_3\text{Te}_3 + \beta$ crystallize.

The determination of the microhardness of alloys in the Sb_2Te_3 – InSe system gave four different values: 860–890 MPa corresponds to the α -phase of the solid solutions based on Sb_2Te_3 ; 900–930 MPa, to the new phase $\text{InSb}_2\text{SeTe}_3$; 1210 MPa, to the new phase $\text{In}_3\text{Sb}_2\text{Se}_3\text{Te}_3$; and 600–700 MPa, to the β -solid solutions based on InSe .

The temperature dependences of the electrical conductivity (Fig. 5) and thermal emf (Fig. 6) of the solid solutions $(\text{Sb}_2\text{Te}_3)_{1-x}(\text{InSe})_x$ ($x = 0.01, 0.02$, and 0.03) were measured in the temperature range 25– 400°C . It was revealed that, in the low-temperature range (25– 225°C), the conduction of the solid solutions is metallic, and in the high-temperature range (225°C and higher), the solid solutions are semiconductors.

The electrical conductivity of the alloys of the solid solutions $(\text{Sb}_2\text{Te}_3)_{1-x}(\text{InSe})_x$ containing 1, 2, and 3 mol % InSe , depending on the composition,

**Fig. 2.** (a) Spectra and (b) microstructure of the compound $\text{InSb}_2\text{SeTe}_3$ according to scanning electron microscopy data.

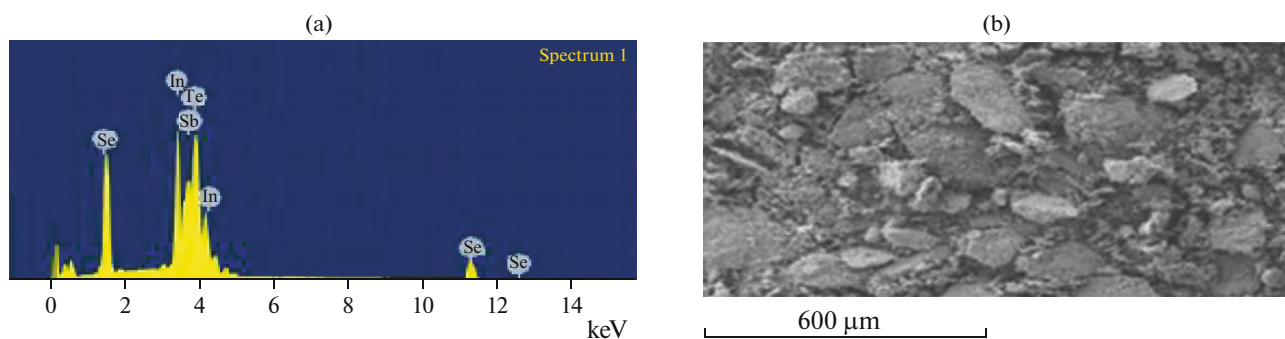


Fig. 3. (a) Spectra and (b) microstructure of the compound $\text{In}_3\text{Sb}_2\text{Se}_3\text{Te}_3$ according to scanning electron microscopy data.

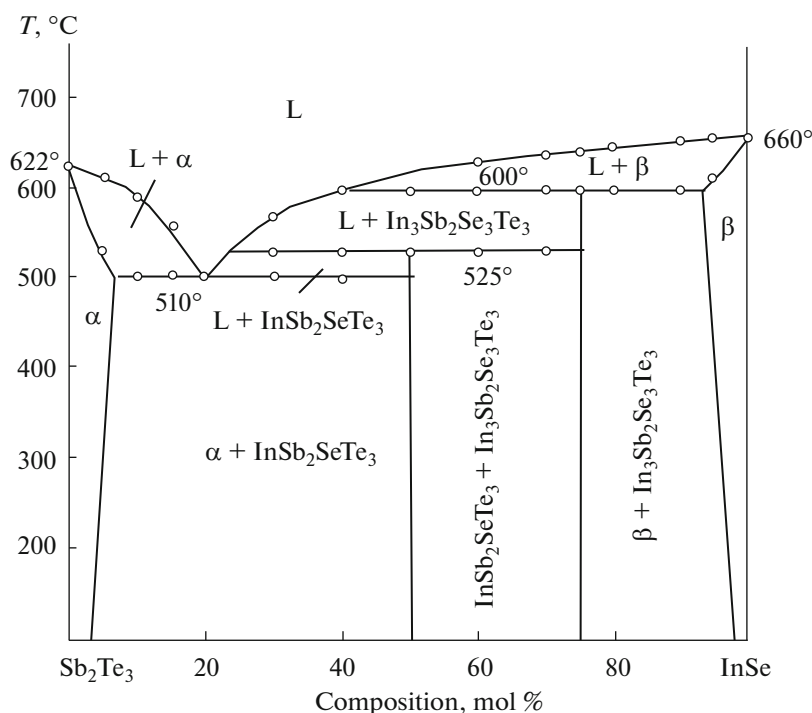


Fig. 4. T - x phase diagram of the Sb_2Te_3 - InSe system.

increases from $\sigma = 120 \times 10^3$ to 137×10^3 and to $150 \times 10^3 \Omega^{-1} \text{cm}^{-1}$. The temperature dependence of the electrical conductivity of the alloys containing 1, 2, and 3 mol % InSe corresponds to the metallic conduction; therefore, the electrical conductivity initially decreases to 500 K, and with a further increase in temperature, the conduction becomes intrinsic, and the electrical conductivity of the alloys containing 1, 2, and 3 mol % InSe increases.

Figure 6 presents the temperature dependence of the thermal emf of the solid solutions $(\text{Sb}_2\text{Te}_3)_{1-x}(\text{InSe})_x$ ($x = 0.01, 0.02, \text{ and } 0.03$). This dependence is seen to have an extremum: from room temperature to $\sim 180^\circ\text{C}$, the thermal emf increases, and at high temperatures (180 – 400°C), it monotonically decreases.

The dependence $\alpha \sim f(1/T)$, as well as the dependence $\sigma \sim f(1/T)$, can also be divided into two parts. The thermal emf increases with increasing InSe content. It was determined from the sign of the thermal emf that, in the studied temperature range, all the tested alloys of the solid solutions $(\text{Sb}_2\text{Te}_3)_{1-x}(\text{InSe})_x$ ($x = 0.01, 0.02, \text{ and } 0.03$) are p -type semiconductors.

CONCLUSIONS

The Sb_2Te_3 - InSe system was studied over a wide concentration range to characterize the chemical interaction between the components. It was found that the Sb_2Te_3 - InSe system is a quasi-binary eutectic system. Two compounds form in the system at ratios

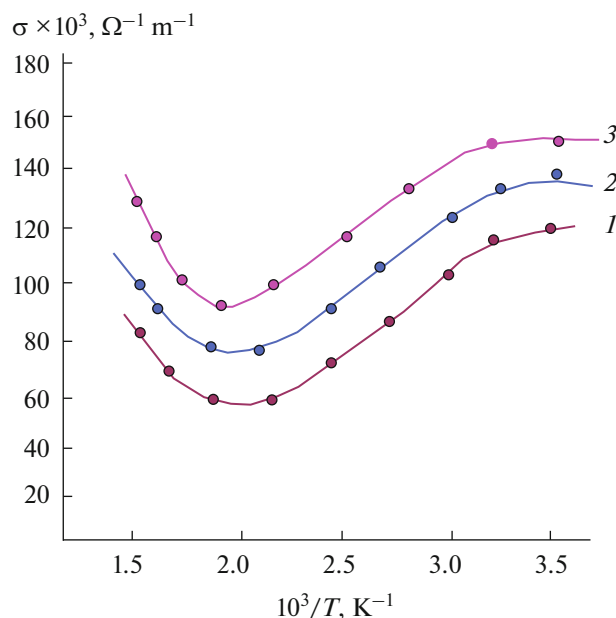


Fig. 5. Temperature dependences of the electrical conductivity of the solid solutions $(\text{Sb}_2\text{Te}_3)_{1-x}(\text{InSe})_x$ at (1) 1, (2) 2, and (3) 3 mol % InSe.

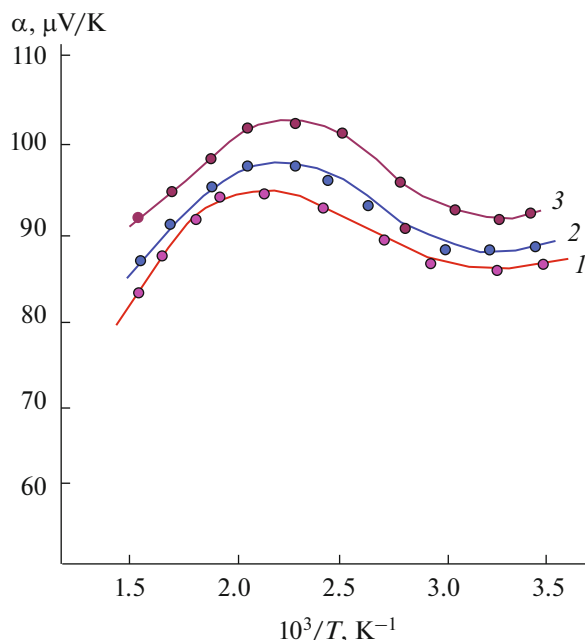


Fig. 6. Temperature dependences of the thermal emf of the solid solutions $(\text{Sb}_2\text{Te}_3)_{1-x}(\text{InSe})_x$ at (1) 1, (2) 2, and (3) 3 mol % InSe.

between the components of 1 : 1 and 1 : 3 by the peritectic reactions $\text{L} + \text{InSe} \leftrightarrow \text{InSb}_2\text{SeTe}_3$ (525°C) and $\text{L} + \text{InSb}_2\text{SeTe}_3 \leftrightarrow \text{In}_3\text{Sb}_2\text{Se}_3\text{Te}_3$ (600°C).

The results of the microstructural analysis showed the presence of limited regions of solid solutions based

on the initial components at 3 mol % InSe and 2 mol % Sb_2Te_3 . It was determined that, in the concentration range 0–20 mol % InSe, α -phases, i.e., solid solutions based on Sb_2Te_3 , crystallize. The α -phase and $\text{InSb}_2\text{SeTe}_3$ form a eutectic with the coordinates 20 mol % InSe and 510°C . The temperature dependences of the electrical conductivity and thermal emf of alloys of the solid solutions $(\text{Sb}_2\text{Te}_3)_{1-x}(\text{InSe})_x$ ($x = 0.01, 0.02, \text{ and } 0.03$) were investigated. It was determined from the sign of the electrical conductivity and thermal emf that, in the studied temperature range, all the tested alloys of the solid solutions $(\text{Sb}_2\text{Te}_3)_{1-x}(\text{InSe})_x$ ($x = 0.01, 0.02, \text{ and } 0.03$) are p -type semiconductors.

CONFLICT OF INTEREST

The authors declare no conflict of interest.

REFERENCES

1. V. A. Petrusevich and V. M. Sergeeva, *Fiz. Tverd. Tela* **2**, 2858 (1960).
2. E. L. Zorina and T. N. Guliev, *Opt. Spektrosk.* **22**, 919 (1967).
3. B. T. Kolomiets and S. M. Ryvkin, *Zh. Tekh. Fiz.* **19**, 2041 (1974).
4. D. P. Belotskii, P. F. Babyuk, and N. V. Demyanchuk, in *Low-Temperature Thermoelectric Materials* (Inst. Appl. Phys., Akad. Nauk Mold. SSR, Akad. Nauk SSR, Kishinev, 1970), p. 29 [in Russian].
5. A. I. Zaslavskii, V. M. Sergeeva, and I. A. Smirnov, *Fiz. Tverd. Tela* **2**, 2885 (1960).
6. A. G. Kyazym-zade, A. A. Agaeva, V. M. Salmanov, and A. G. Mokhtari, *Zh. Tekh. Fiz.* **7** (4), 80 (2007).
7. A. Z. Magomedov, A. O. Aliev, M. A. Aslanov, et al., *Vestn. Bakinskogo Univ. Ser. Fiz.-Mat. Nauki* **7** (4), 163 (2004).
8. A. Z. Magomedov, L. G., A. O. Aliev, et al., *Fizika* **13** (4), 164 (2007).
9. R. Zybala, K. Mars, A. Mikula, et al., *Arch. Metall. Mater.* **62** (2B), 1067 (2017).
<https://doi.org/10.1515/amm-2017-0155>
10. A. M. Fernandez and M. G. Merino, *Thin Solid Films* **366** (1–2), 202 (2000).
11. T. E. Svechnikova, L. E. Shelimova, P. P. Konstantinov, et al. *Inorg. Mater.* **42**, 1311 (2006).
12. E. M. F. Vieira, J. Figueira, A. L. Pires, et al., *J. Alloys Compd.* **774**, 1102 (2019).
<https://doi.org/10.1016/j.jallcom.2018.09.324>
13. Bin Xu, Jing Zhang, Gongqi Yu, et al., *J. Appl. Phys.* **124**, 165104 (2018).
<https://doi.org/10.1063/1.5051470>
14. V. A. Kulbachinskii, V. G. Kytin, D. A. Zinoviev, et al., *Semiconductors* **53**, 638 (2019).
<https://doi.org/10.1134/S1063782619050129>
15. P. Parekh and P. T. Chiang, *Alloys Can. J. Phys.* **43**, 653 (2011).
<https://doi.org/10.1139/p65-060>

16. Min Ho Lee, Ka-Ryeong Kim, Jong-Soo Rhyee, et al., *J. Mater. Chem. C* **3**, 10494 (2015).
<https://doi.org/10.1039/C5TC01623A>
17. S. Morikawa, T. Inamoto, and M. Takashiri, *Nanotechnology* **9** (7), 075701 (2018).
<https://doi.org/10.1088/1361-6528/aaa31f>
18. Xiao-Yu Wang, Hui-Juan Wang, Bo Xiang, et al., *ACS Appl. Mater. Interfaces* **10** (27), 23277 (2018).
<https://doi.org/10.1021/acsami.8b01719>
19. I. B. Bakhtiyarly, R. A. Ismailylova, and V. A. Gasymov, et al., *Russ. J. Inorg. Chem.* **54**, 1820 (2009).
20. I. I. Aliev, R. S. Magammedragimova, O. M. Aliev, and K. N. Babanly, *Russ. J. Inorg. Chem.* **64**, 527 (2019).
<https://doi.org/10.1134/S003602361904003X>
21. F. M. Sadygov, T. M. Il'yasly, G. T. Ganbarova, et al., *Inorg. Mater.* **53**, 665 (2017).
22. F. M. Sadygov, S. G. Mamedova, M. B. Babanly, and T. M. Il'yasov, *Russ. J. Inorg. Chem.* **46**, 1247 (2001).
23. A. V. Kertman, *Russ. J. Inorg. Chem.* **64**, 130 (2019).
24. T. F. Maksudova and I. I., *Russ. J. Inorg. Chem.* **48**, 425 (2003).
25. M. I. Zargarova, A. N. Mamedov, D. S. Azhdarova, et al. *Inorganic Substances Synthesized and Studied in Azerbaijan: A Handbook* (ELM, Baku, 2004) [in Russian].
26. Haixu Qin, Jianbo Zhu, Bo Cui, et al., *ACS Appl. Mater. Interfaces* **12**, 945 (2020).
<https://doi.org/10.1021/acsami.9b19798>
27. N. Kh. Abrikosov, V. F. Bankina, L. V. Proetsskaya, et al., *Semiconductor Chalcogenides and Alloys Based on Them* (Nauka, Moscow, 1975).
28. D. H. Donnay and H. M. Ondik, *U.S. Comm. Nat. Bur. Stand. and Joint. Commit. Powd. Diff. Stand.* **2**, 1902 (1973).
29. V. G. Kuznetsov and K. K. Palkina, *Zh. Neorg. Khim.* **8**, 1204 (1963).
30. *State Diagrams of Binary Metal Systems*, Ed. by N.P. Lyakishev (Mashinostroenie, Moscow, 2001), Vol. 3 [in Russian].
31. N. B. Kolomiets, *Zavod. Lab.* **28** (2), 238 (1962).

Translated by V. Glyanchenko